

## **Chapter 3 - Eddies along the western boundary of the Bay of Bengal**

### **3.1. Introduction**

The western boundary of the BOB was sampled three times during summer (22 to 30 of July 2001), fall intermonsoon (30 September to 11 October 2002) and spring intermonsoon (27 April to 5 May 2003). The seasonal variability of the thermohaline structure along the western boundary of the OB was examined to decipher the occurrence of eddies and its spatio-temporal characteristics. For this purpose the sequence of seasons rather than year is followed in explaining the observed features along the western Bay of Bengal. Cyclonic and anticyclonic eddies are characterized by doming and depressions in the thermohaline structure. These domings and depressions along with the geostrophic velocities computed w.r.t 1000 m is used for the identification of eddies from the hydrography. Further, sea-level anomalies from satellite altimeter are used to confirm observed features and to track its evolution with time.

### **3.2. Thermohaline structure**

#### **3.2.1 Spring intermonsoon 2003**

Thermal structure showed a warmer and thicker isothermal layer with upper waters in excess of 30°C in the south, south of 16°N (Figure 3.2.1.1a). Towards the north the isothermal layer was shallower and about 1°C colder. Important features of the thermal structure were the doming of isotherms centered at 14°N and 18°N respectively and a depression centered at 15.5°N. The doming was more pronounced in the deeper layers (below 250 m) in the former case, while that for the latter was in the upper thermocline

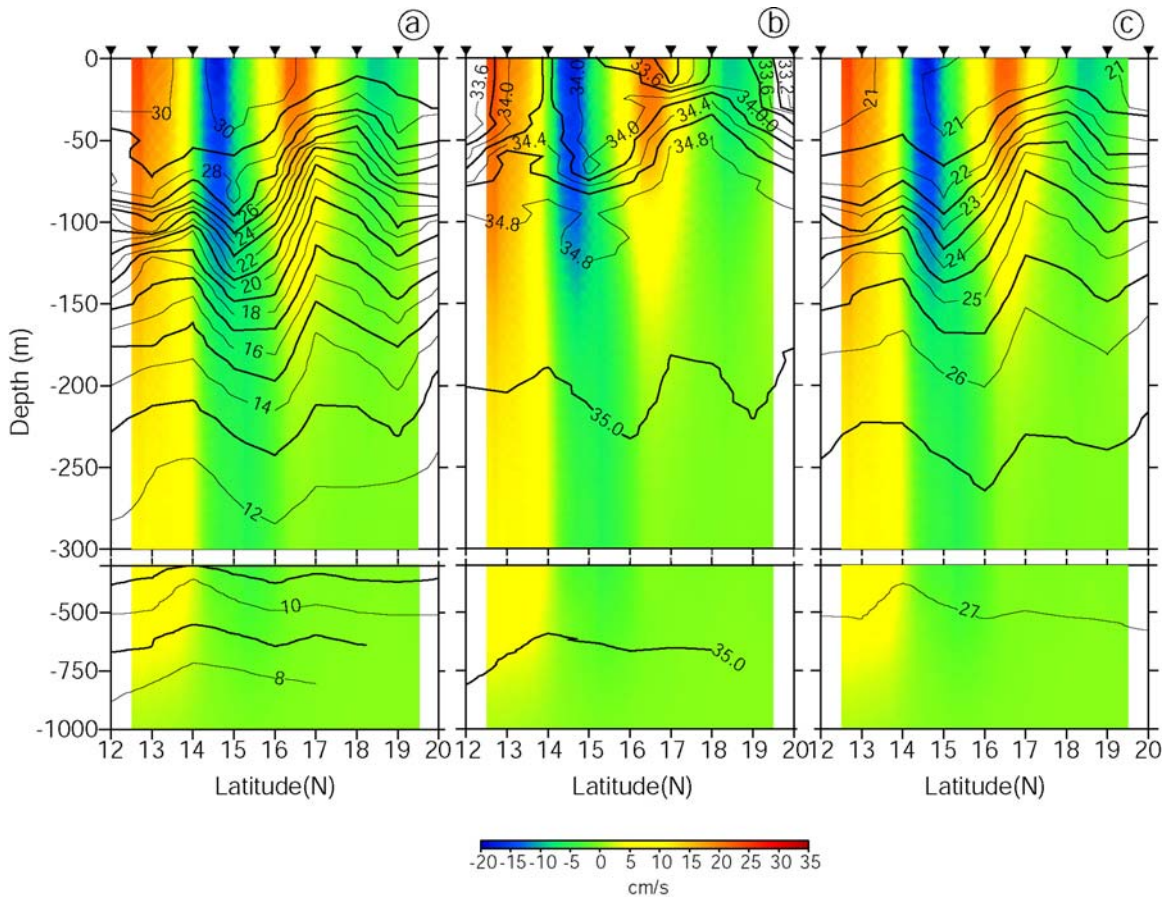


Figure 3.2.1.1 Vertical sections of (a) temperature ( $^{\circ}\text{C}$ ), (b) salinity (psu), and (c) sigma-t ( $\text{kg}/\text{m}^3$ ) overlaid on the geostrophic velocity ( $\text{cm}/\text{s}$ ) w.r.t 1000 m along the western boundary in the BOB during spring intermonsoon (April-May) 2003. Filled inverted triangles indicate the position of CTD stations.

(upper 250 m). For example, the  $10^{\circ}\text{C}$  isotherm shoaled by about 150 m in the former case, while it was only about 30 m for the latter. On the contrary the  $20^{\circ}\text{C}$  isotherm shoaled maximum, by about 75 m, in the latter case and it was only less than 30 m for the former. In the case of the depression  $20^{\circ}\text{C}$  isotherm was depressed by about 30 m. The doming centered at  $14^{\circ}\text{N}$  and  $18^{\circ}\text{N}$  depressed the ambient temperature at 100 m by  $3^{\circ}\text{C}$  and  $6^{\circ}\text{C}$  respectively, whereas the depression increased the temperature by one degree. The salinity distribution also reflected features similar to that of temperature with higher salinity,  $\sim 34$  psu (practical salinity unit), in the south and about 0.5 psu fresher towards the north (Figure 3.2.1.1b). Consistent with thermal structure, isohalines also showed

doming which was visible only below 50 m centered at 14°N but was evident even at 20 m centered at 18°N. The doming of isohaline at 14°N and 18°N increased the salinity at 50 m by 0.4 psu and 0.8 psu respectively. The 34 psu contour was pushed down to a depth of about 75 m in the center of the depression. The density ( $\sigma_t$ ) distribution (Figure 3.2.1.1c) essentially reflected a structure similar to that of temperature and salinity.

The geostrophic velocities computed w.r.t 1000 m from the hydrographic data revealed an eastward current south of 14°N attaining a maximum velocity of 30 cm/s followed by a weak westward flow with a peak value of 20 cm/s towards the north up to 16°N (Figure 3.2.1.1 shading). Once again eastward and westward velocities were encountered at the southern and northern side of 18°N respectively. The westward currents, however, were much smaller (~10 cm/s) in the later case. These opposing flows and the doming in the property distribution appear to be a part of the cyclonic circulation feature centered at 14°N and 18°N respectively along the western boundary.

### **3.2.2. Summer Monsoon 2001**

The prominent feature of the thermohaline structure during summer was the up/down sloping of isolines centered at 17°N (Figure 3.2.2.1.a, b), as in the case of spring intermonsoon, except that the center appears to be shifted southward from its spring position of 18°N. The up-down sloping of isotherm/isohaline noticed in the upper 150 m at 14°N during spring intermonsoon completely disappeared in summer monsoon. However, below 150 m, thermal structure still showed feature similar to Spring intermonsoon. It is clear from the thermohaline structure that the upper layer was

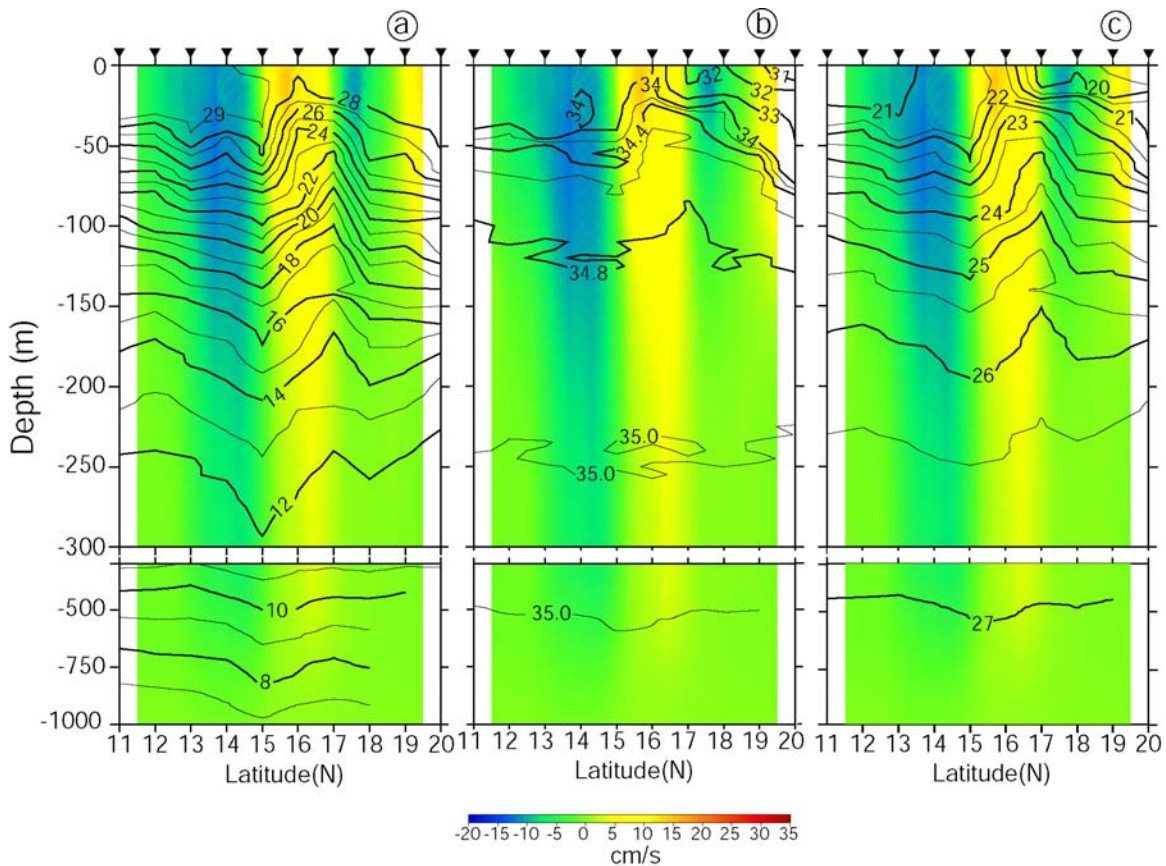


Figure 3.2.2.1 Vertical sections of (a) temperature ( $^{\circ}\text{C}$ ), (b) salinity (psu), and (c) sigma-t ( $\text{kg}/\text{m}^3$ ) overlaid on the geostrophic velocity ( $\text{cm}/\text{s}$ ) w.r.t 1000 m along the western boundary in the BOB during summer (July-August) 2001. Note the change in contour interval  $<33$  psu in (b), which is 1 psu. Filled inverted triangles indicate the position of CTD stations.

modified by the presence of the eddy. The isothermal layer which was on an average 30 m deep along the track came very close to the surface under the influence of the eddy centered at  $17^{\circ}\text{N}$ . Though SST along the track was  $1^{\circ}\text{C}$  colder than spring intermonsoon, it retained the spatial pattern with colder SST in the north. During summer monsoon too the  $20^{\circ}\text{C}$  isotherm underwent a maximum displacement, but the magnitude was much less ( $\sim 40$  m). Similarly the eddy depressed the ambient temperature at 100 m by about  $3^{\circ}\text{C}$  which was half that during Spring intermonsoon. Consistent with the thermal structure, isohalines too domed centered around  $17^{\circ}\text{N}$  (Figure 3.2.2.1b). This resulted in the increase of salinity at 50 m by about 0.4 psu at the centre of the eddy. The conspicuous

feature in the haline structure was the presence of fresher waters ( $\sim 30$  psu) in the northern part and the strong vertical gradient of about 4 psu in the upper 50 m. However, in the south salinity was close to 34.5 psu in the upper 50 m. The density ( $\sigma_t$ ) distribution (Figure 3.2.2.1c) essentially depicted a structure similar to that of temperature and salinity.

The geostrophic velocities showed westward flow in the southern parts of the transect that peaked ( $\sim 15$  cm/s) at  $14^\circ\text{N}$  (Figure 3.2.2.1 shading) in contrast to spring intermonsoon. North of  $15^\circ\text{N}$  the flow turned eastward with a velocity of approximately 15 cm/s, which gradually slowed down and reached a minimum value at about  $17^\circ\text{N}$ . Once again, the flow increased in its strength to about 10 cm/s in a westward direction at about  $18^\circ\text{N}$ . Thus, from the above a cyclonic flow centered about  $17^\circ\text{N}$  was discernible which roughly coincided with the doming of the isotherm/isohalines/isopycnals indicating the presence of a cyclonic eddy. However, the westward flow south of  $14^\circ\text{N}$ , which replaces the spring-time eastward flow indicated the change in the circulation from cyclonic to anticyclonic. Apart from this, a weak depression centered at  $15^\circ\text{N}$  with an anticyclonic flow field is also noticed in the thermal structure.

### **3.2.3. Fall intermonsoon 2002**

Thermal structure showed that SST, in general, was  $1^\circ\text{C}$  warmer than that in summer monsoon with water of about  $30^\circ\text{C}$  occupying most of the region along the transect except north of  $18^\circ\text{N}$  (Figure 3.2.3.1a). Here again, the conspicuous feature was two domes of isotherms centered at  $12^\circ\text{N}$  and  $18^\circ\text{N}$  respectively. The  $20^\circ\text{C}$  isotherm had undergone maximum displacement of 50 m for the latter, while it was only about 20 m

for the former. On the contrary, the 10°C isotherm underwent a maximum displacement of nearly 100m in the former case, while the latter did not show appreciable change. This indicated that the feature at 18°N was prominent in the upper layers of the water column with not much variability below the thermocline. However, the feature at 12°N was though discernible in the upper thermocline, was most prominent in the deeper layers and extended up to 1000 m. Accordingly, the ambient temperature at 100 m was depressed by about 1°C and 4°C respectively. Vertical section of salinity showed the presence of very low salinity waters (~23 psu) in the north and the effect of freshening was felt as south as 14°N (Figure 3.2.3.1b). This increased the vertical gradient of salinity in the upper 50 m by about 10 psu in the north. The effect of eddy could be inferred from the doming isohaline, which increased the ambient salinity at 50 m by about 1 psu and 0.4 psu for eddies centered at 18°N and 12°N respectively. During fall intermonsoon the eddy was completely overlaid by this freshwater. Thus, the fresh water severely constrained the eddy pumping of saltier waters from subsurface and thereby restricting the eddy signature below the surface layer (below ~15 m). The density ( $\sigma_t$ ) structure also reflected features of temperature and salinity fields (Figure 3.2.3.1c).

Geostrophic velocities showed alternate bands of positive (eastward) and negative (westward) flows all along the track (Figure 3.2.3.1 shading). At 11°N the flow was eastward with a velocity of 15 cm/s, which gradually decreased to a minimum at 12°N and turned to a westward flow of magnitude 15 cm/s centered 13°N. The current once again changed direction towards east at 17°N with its speed decreasing to a minimum at 18°N, followed by another change in direction towards west and increase in its strength



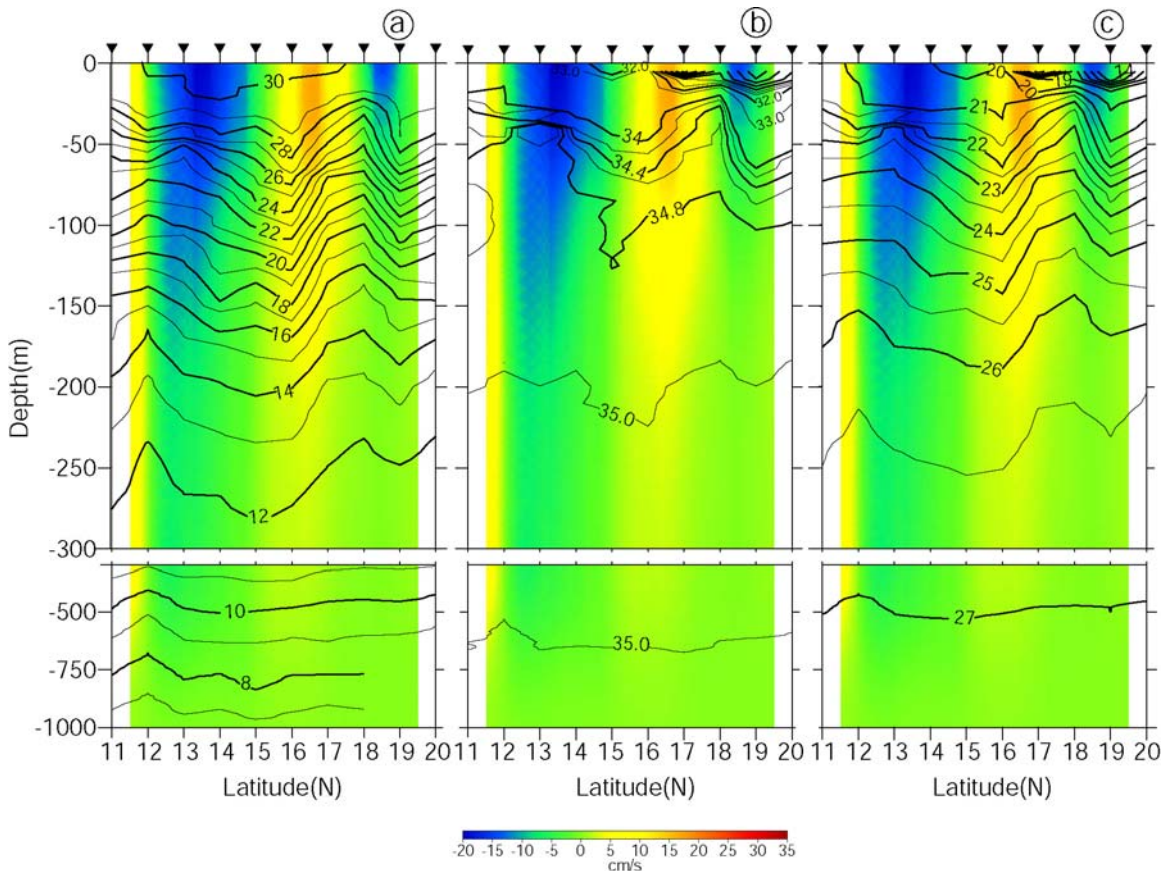


Figure 3.2.3.1 Vertical sections of (a) temperature ( $^{\circ}\text{C}$ ), (b) salinity (psu), and (c) sigma-t ( $\text{kg}/\text{m}^3$ ) overlaid on the geostrophic velocity (cm/s) w.r.t 1000 m along the western boundary in the BOB during fall intermonsoon (September-October) 2002. Note the change in contour interval  $<34$  psu in (b), which is 1 psu and  $<21$   $\text{kg}/\text{m}^3$  in c which is 1  $\text{kg}/\text{m}^3$ . Filled inverted triangles indicate the position of CTD stations.

to about 15 cm/s at  $19^{\circ}\text{N}$ . Thus, from the flow pattern the signatures of two cyclonic eddies centered about  $12^{\circ}\text{N}$  and  $18^{\circ}\text{N}$  along the track was discernible, though in the thermohaline structure only the northern eddy was most visible in the upper layers. During this season too a weak depression and associated anticyclonic flow was noticed in the thermal haline structure centered about  $16^{\circ}\text{N}$ .

Thus, the most prominent feature of the thermohaline structure, in all the three seasons, was the signature of sub-surface cyclonic eddy observed in the northern part of the

western Bay of Bengal (16-19°N). This is designated northern coastal eddy (NCE). A cyclonic eddy during spring and fall intermonsoons in the southern part centered at 14°N and 12°N respectively was also noticed. This has been designated as southern coastal eddy (SCE). A comparison with the sea-level anomaly showed that the depression noticed during the spring intermonsoon was a part of the large scale anticyclonic circulation whereas the one during summer monsoon and fall intermonsoon are anticyclonic eddies.

### **3.3. Evolution of the northern and southern coastal eddy (NCE, SCE) from sea-level anomaly**

Having analyzed the thermohaline structure and identified signatures of eddies from them, it is important to attempt to understand the time evolution of these features in relation to the prevailing circulation. Towards this, seven-day snap shots of the sea-level anomaly maps of the respective years along with the geostrophic flows computed from them were analyzed. Though the sea-level anomaly maps showed several circulation features, the focus of this study is on the NCE and SCE as these were the most dominant feature reflected in the vertical thermohaline structure as well as the geostrophic currents computed from hydrography.

#### **3.3.1. Spring Intermonsoon 2003**

Sea-level anomaly pictures showed a small meander in the northeastward western boundary current (WBC), close to the coast at about 17°N, 84°E during early February 2003 (Figure 3.3.1.1), which developed into an elongated cyclonic flow centered at 16°N,



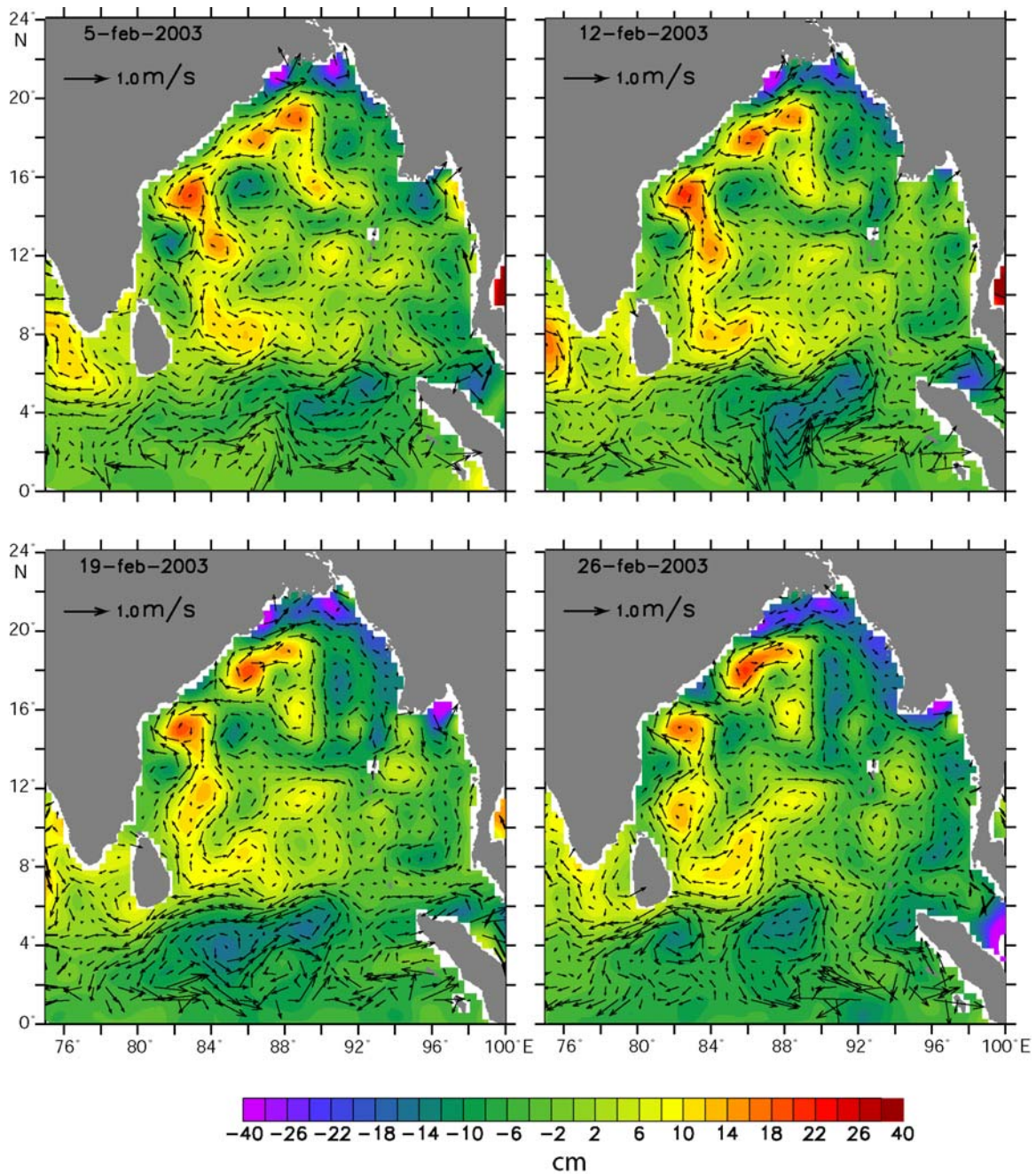


Figure 3.3.1.1 7-day snap-shots of Topex/Poseidon ERS1/2 merged sea-level anomalies overlaid with geostrophic velocities during February 2003.

84.5°E by the last week of March (Figure 3.3.1.2). This cyclonic eddy (NCE) moved onshore, to about 17°N, 84°E by the third week of April (Figure 3.3.1.3) and was sampled from onboard the ship during the last week of April (Figure 3.3.1.4, see Figure 3.2.1.1 for its thermohaline structure). During this period, the eddy was characterized by a negative

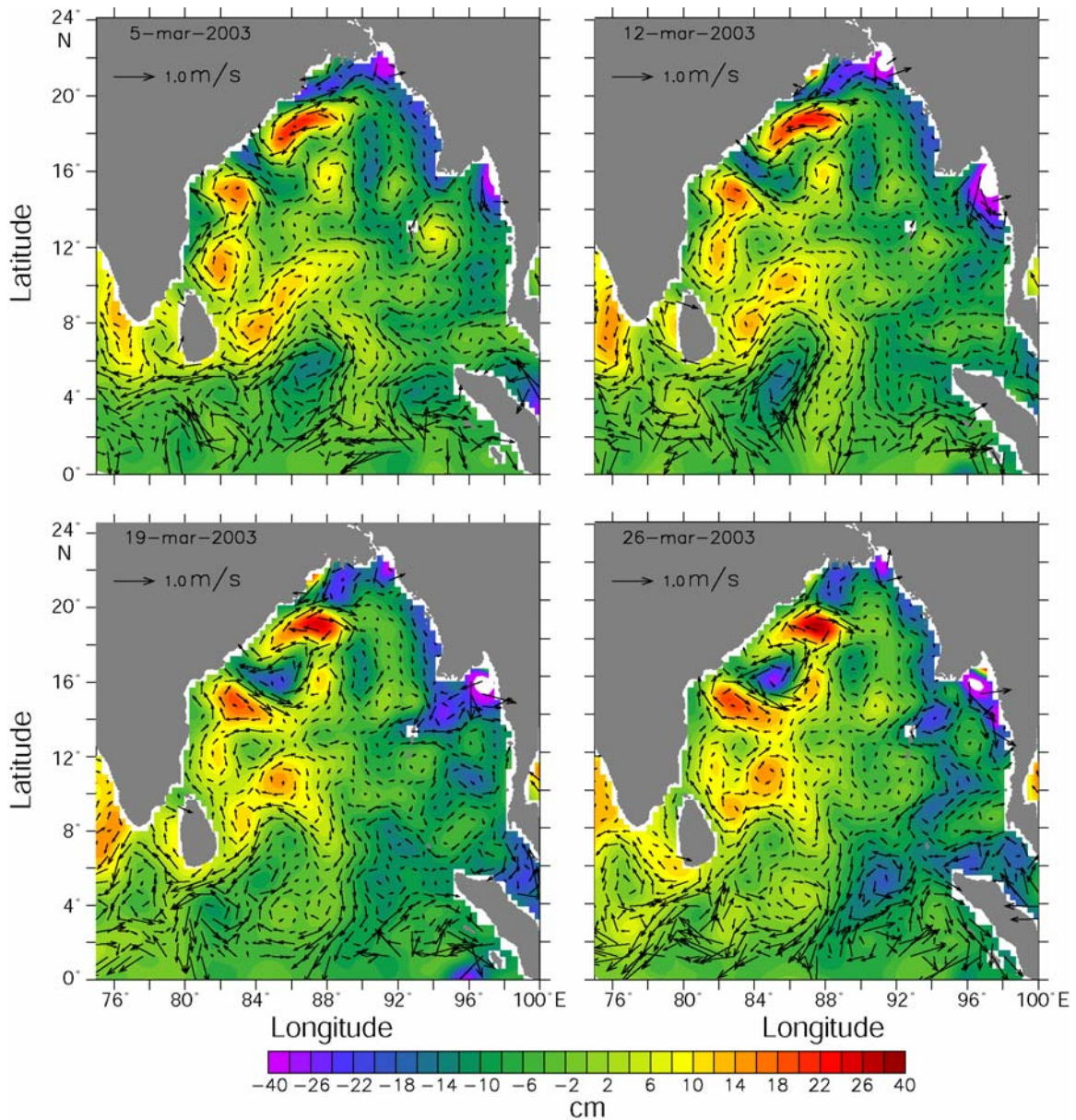


Figure 3.3.1.2. 7-day snap-shots of Topex/Poseidon ERS1/2 merged sea-level anomalies overlaid with geostrophic velocities during March 2003.

sea-level anomaly of about 22 cm and geostrophic velocity of about 30-40 cm/s along its periphery. Subsequently, as the circulation weakened, the eddy moved offshore and coalesced with another cyclonic eddy, by end of May, thereby increasing its strength (Figure 3.3.1.4, bottom right).



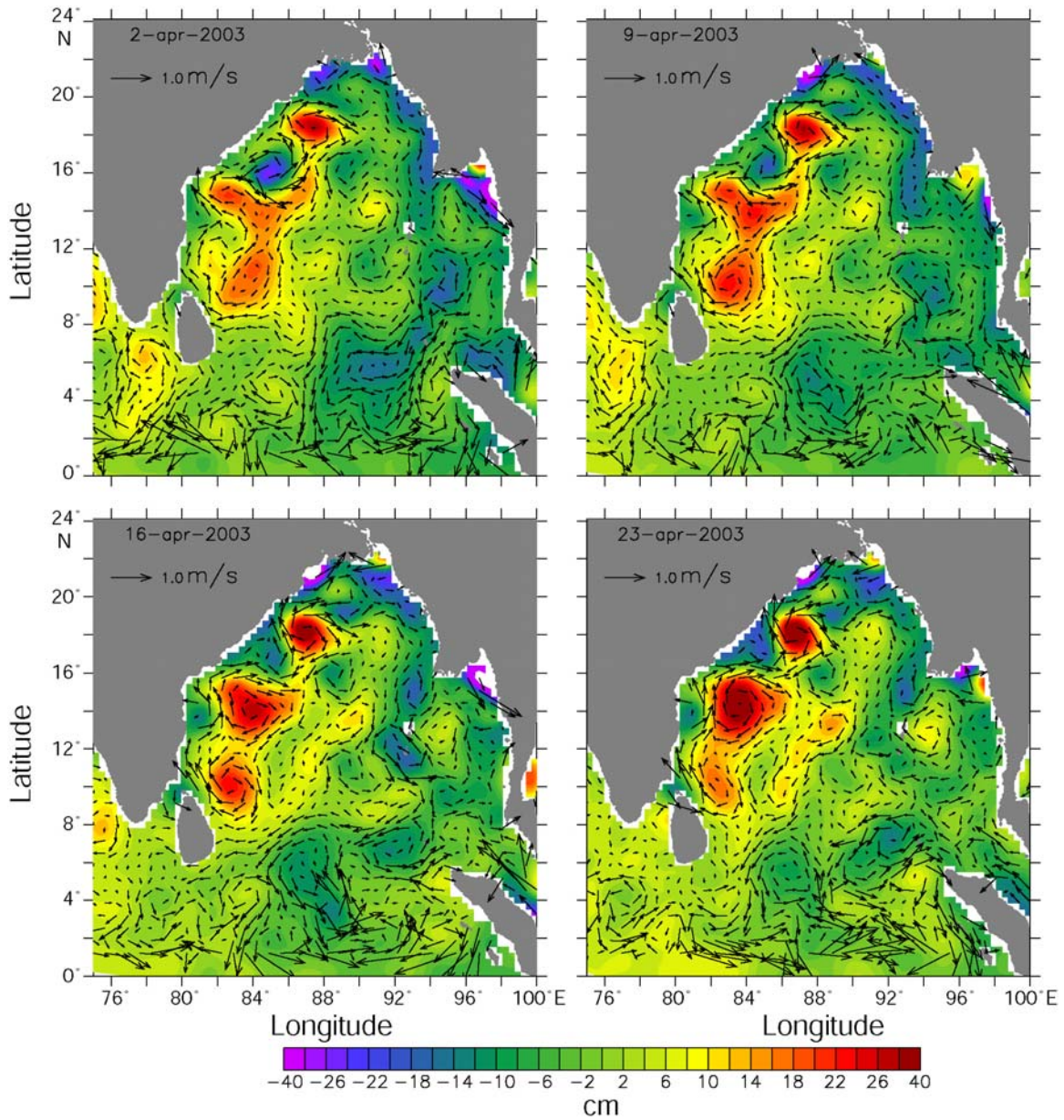


Figure 3.3.1.3. 7-day snap-shots of Topex/Poseidon ERS1/2 merged sea-level anomalies overlaid with geostrophic velocities during April 2003.

In the southern part of the western boundary another cyclonic circulation centered at 13.5°N and 81°E is noticed, which formed in the first week of April (Figure 3.3.1.3).

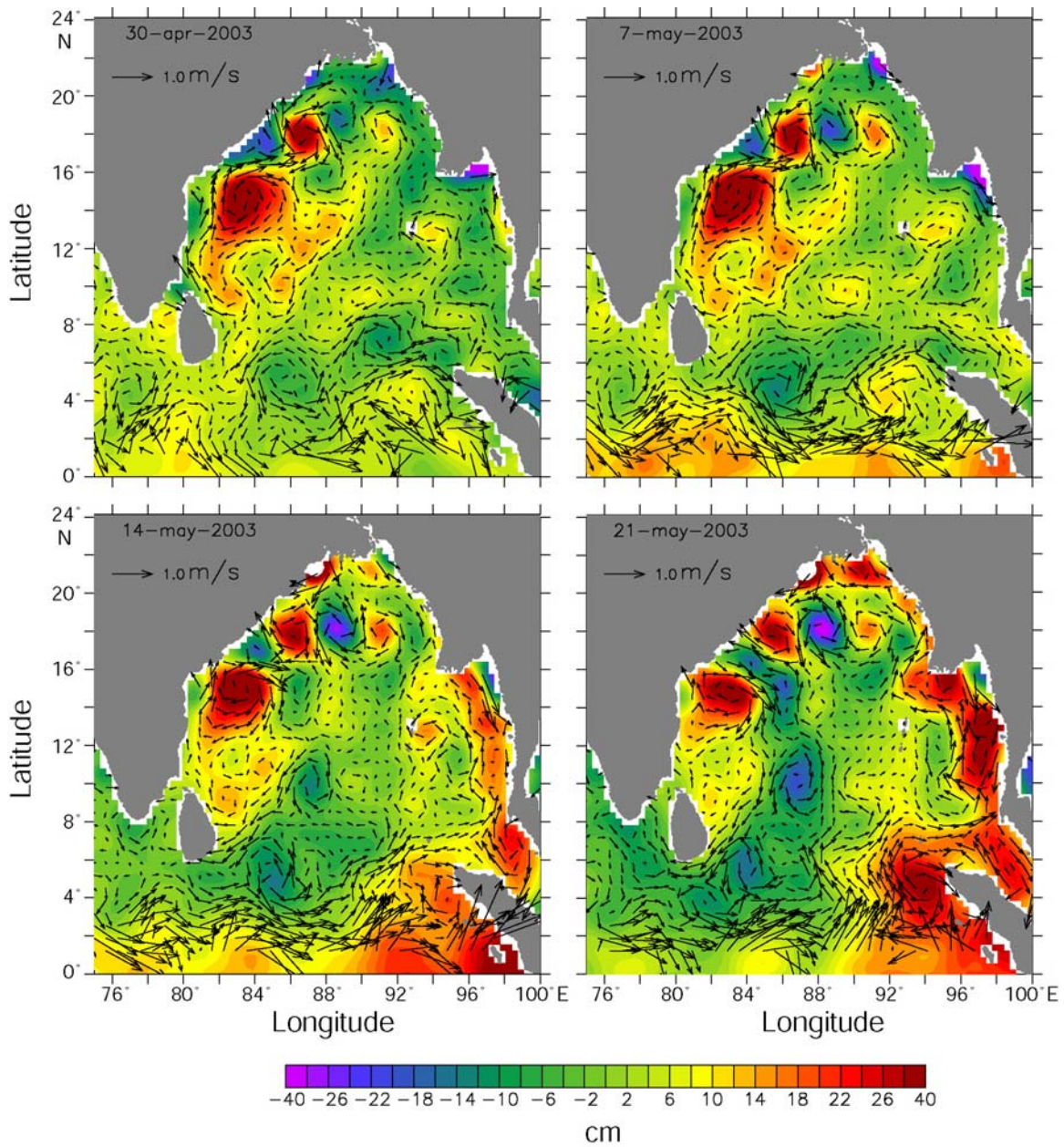


Figure 3.3.1.4. 7-day snap-shots of Topex/Poseidon ERS1/2 merged sea-level anomalies overlaid with geostrophic velocities during April-May 2003.

After persisting for two weeks, it dissipated by the end of April (Figure 3.3.1.4). It is this cyclonic circulation (SCE) that was captured during last week of April 2003 in the hydrographic section centered at 14°N along the western boundary.



### 3.3.2. Summer monsoon 2001

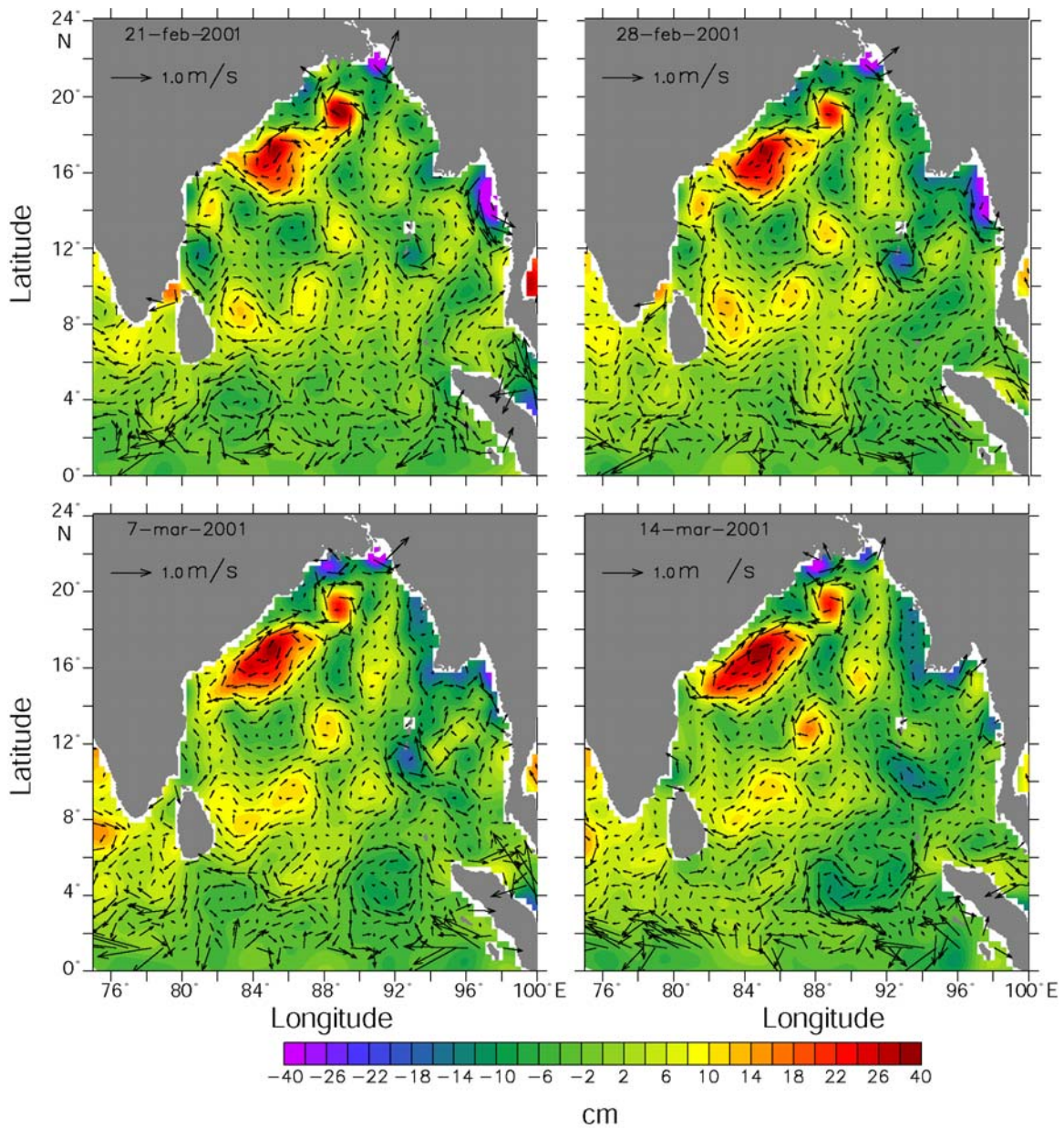


Figure 3.3.2.1. 7-day snap-shots of Topex/Poseidon ERS1/2 merged sealevel anomalies overlaid with geostrophic velocities during February-March 2001.

The eddy observed in summer 2001 (NCE), in the hydrographic section, was also appeared to have formed from a meander in the northeastward current (WBC) during

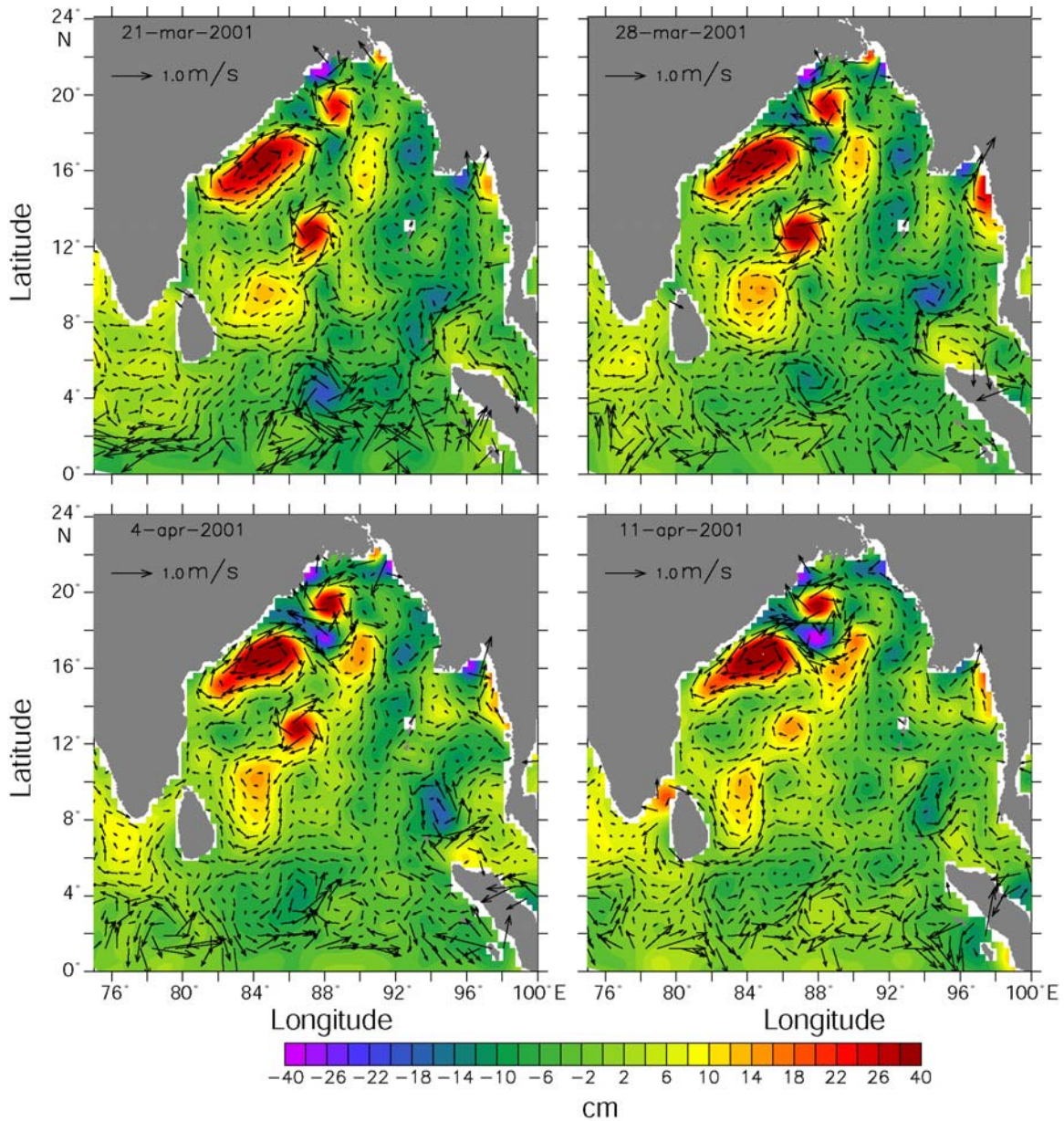


Figure 3.3.2.2. 7-day snap-shots of Topex/Poseidon ERS1/2 merged sealevel anomalies overlaid with geostrophic velocities during March-April 2001.

February (Figure 3.3.2.1) as in the case of 2003 spring intermonsoon eddy. This meander intensified with time and developed into a cyclonic eddy by the end of March 2001 with its centre at  $19^{\circ}\text{N}$ ,  $87^{\circ}\text{E}$  (Figure 3.3.2.2). Another cyclonic eddy was also evident in the sea-level anomaly picture with its centre at  $17.5^{\circ}\text{N}$ ,  $88^{\circ}\text{E}$ . In mid April, these two cyclonic features coalesced and intensified to form a single cyclonic eddy located at



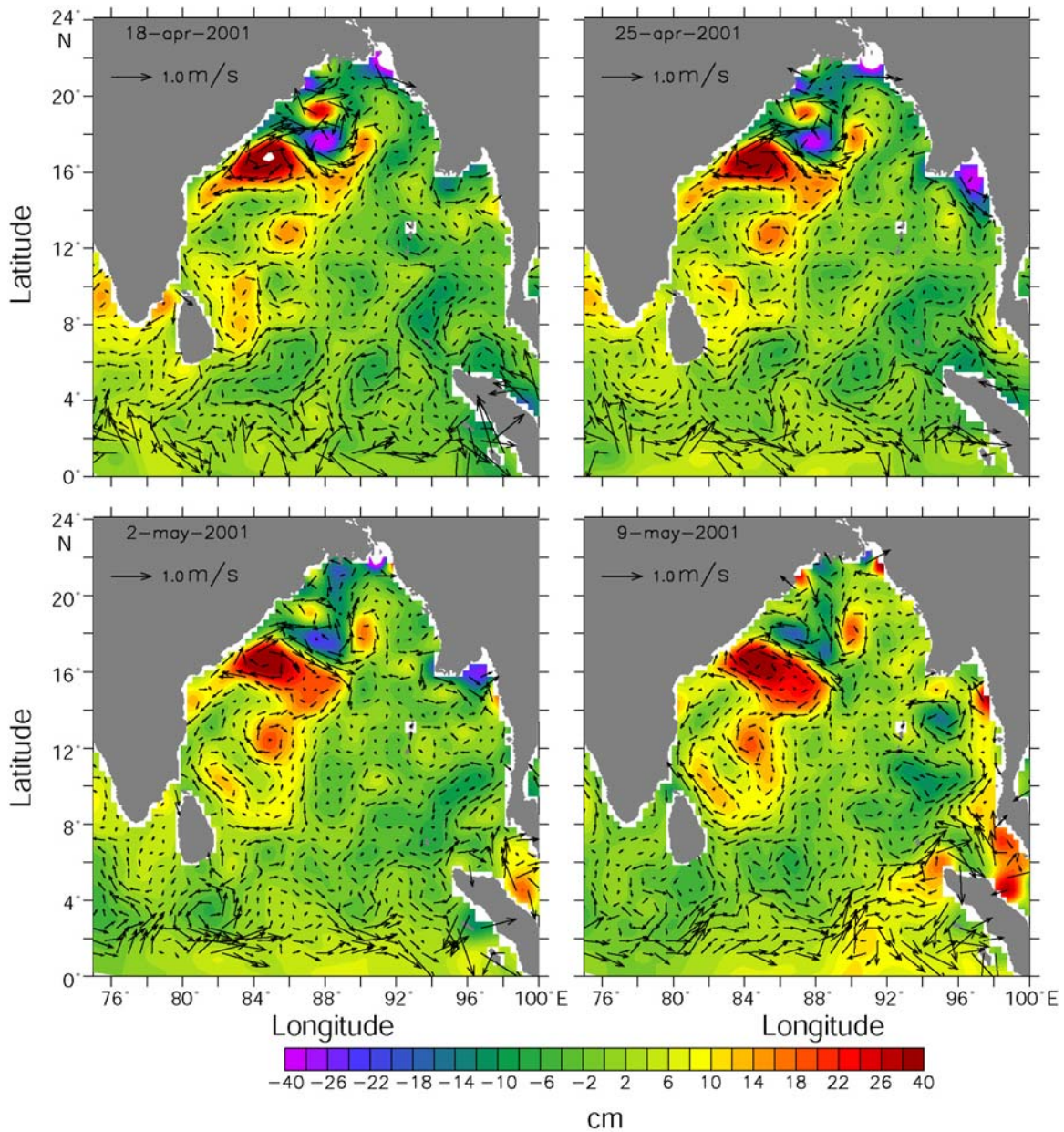


Figure 3.3.2.3. 7-day snap-shots of Topex/Poseidon ERS1/2 merged sealevel anomalies overlaid with geostrophic velocities during April-May 2001.

17.5°N, 88°E (Figure 3.3.2.3). Later, in the second week of May (Figure 3.3.2.4, top left) the single cyclonic eddy split and the northern eddy moved towards the coast while the southern one moved offshore and appeared to coalesce with another weak cyclonic circulation. Subsequently it intensified (Figure 3.3.2.5). During last week of July (Figure 3.3.2.6, bottom left), when the hydrographic measurements were carried out onboard the



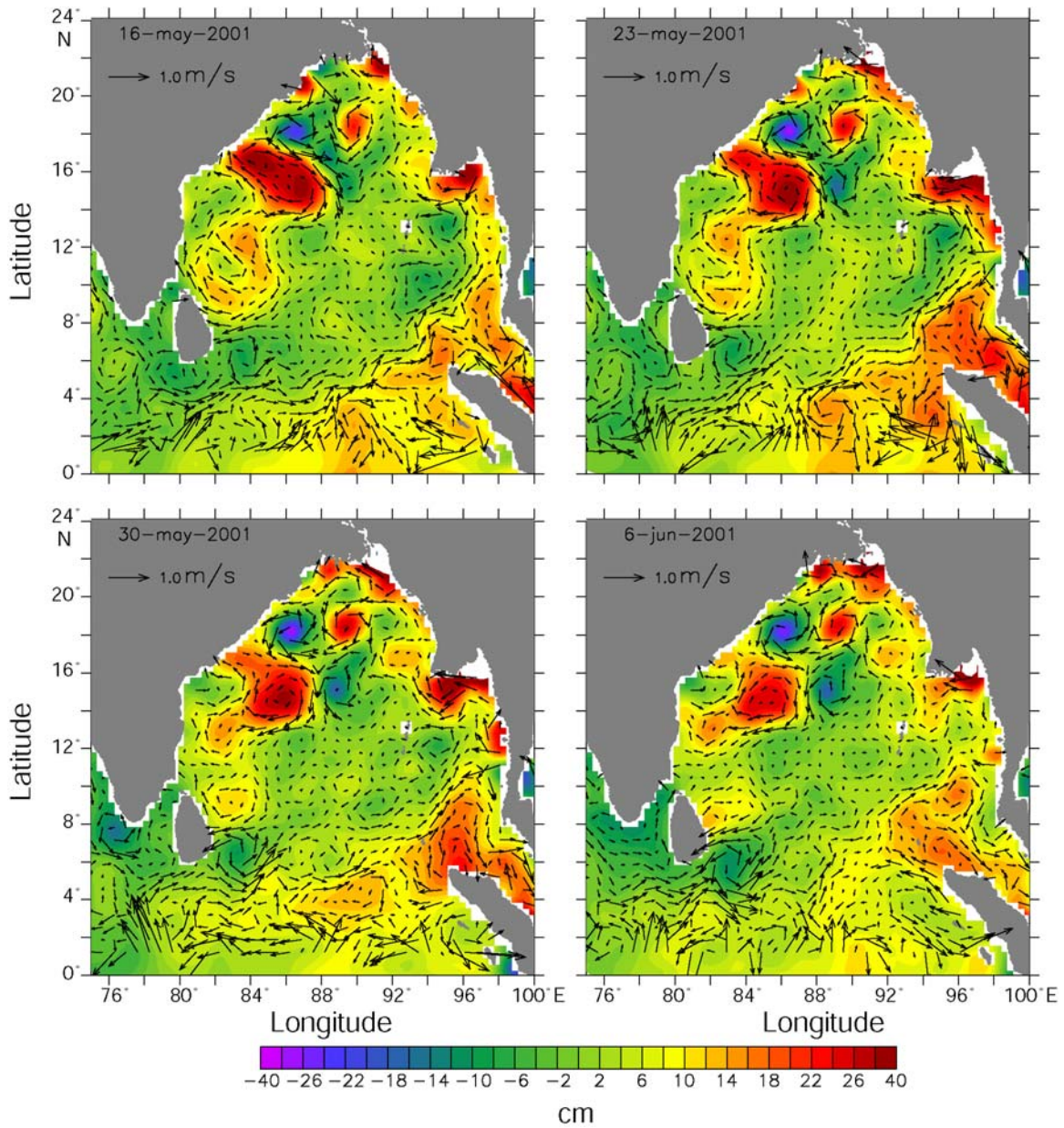


Figure 3.3.2.4. 7-day snap-shots of Topex/Poseidon ERS1/2 merged sealevel anomalies overlaid with geostrophic velocities during May-June 2001.

ship, these two eddies were in a coalesced state and located in a zonal band. Hence the *in situ* measurement picked up the signature of the northern eddy (see Figure 3.2.2.1 for its

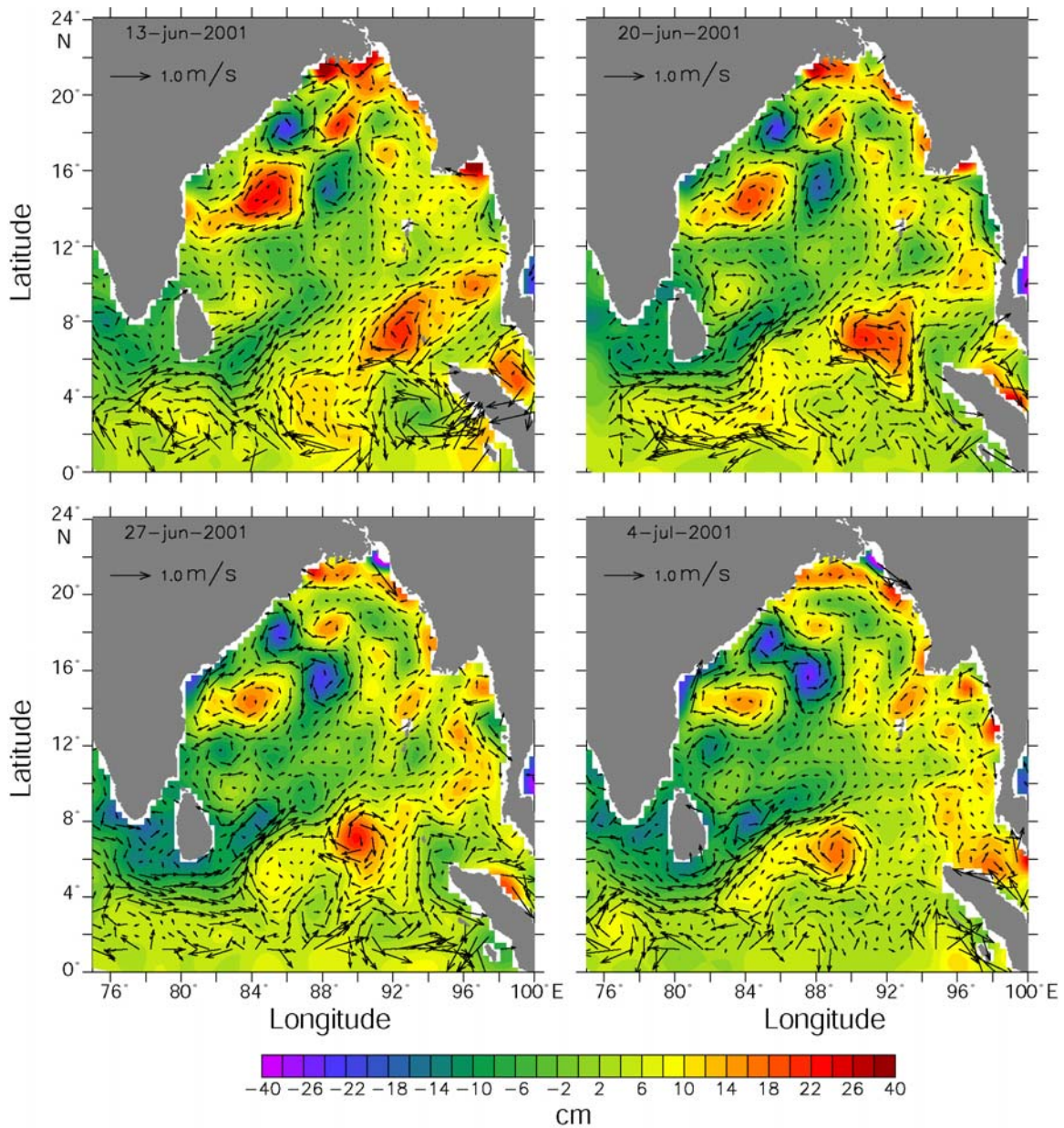


Figure 3.3.2.5 7-day snap-shots of Topex/Poseidon ERS1/2 merged sealevel anomalies overlaid with geostrophic velocities during June-July 2001.

thermohaline structure). The eddy was characterized by a negative sea-level anomaly of 30 cm and geostrophic swirl velocity of 30-40 cm/s along its periphery.



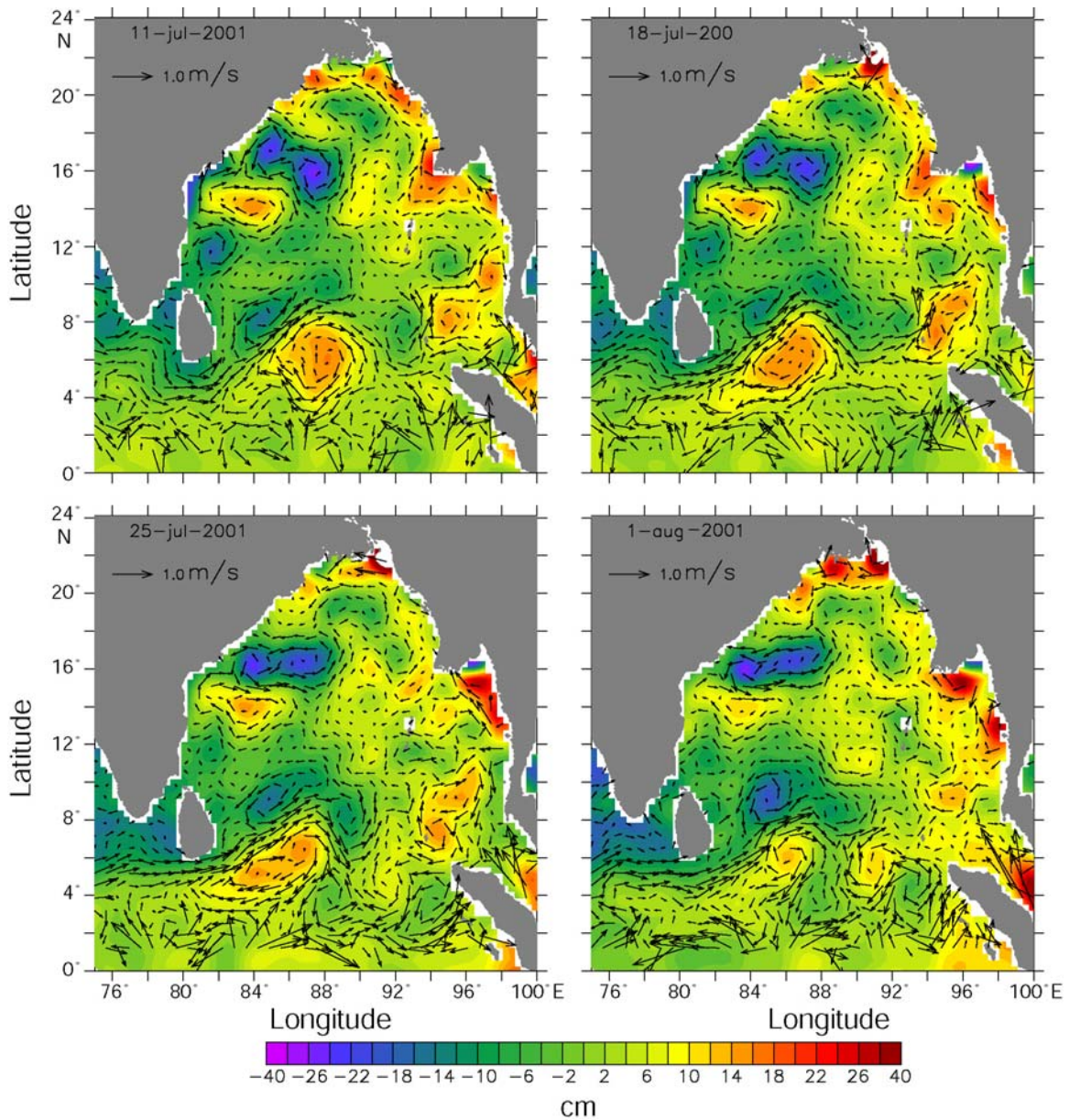


Figure 3.3.2.6. 7-day snap-shots of Topex/Poseidon ERS1/2 merged sealevel anomalies overlaid with geostrophic velocities during July-August 2001.

### 3.3.3. Fall intermonsoon 2002

Unlike the eddy observed during spring intermonsoon and summer monsoon, the fall intermonsoon eddy (NCE) was not developed from the meander in northeastward flowing WBC. The sea-level anomaly picture showed two cyclonic eddies in the first week of

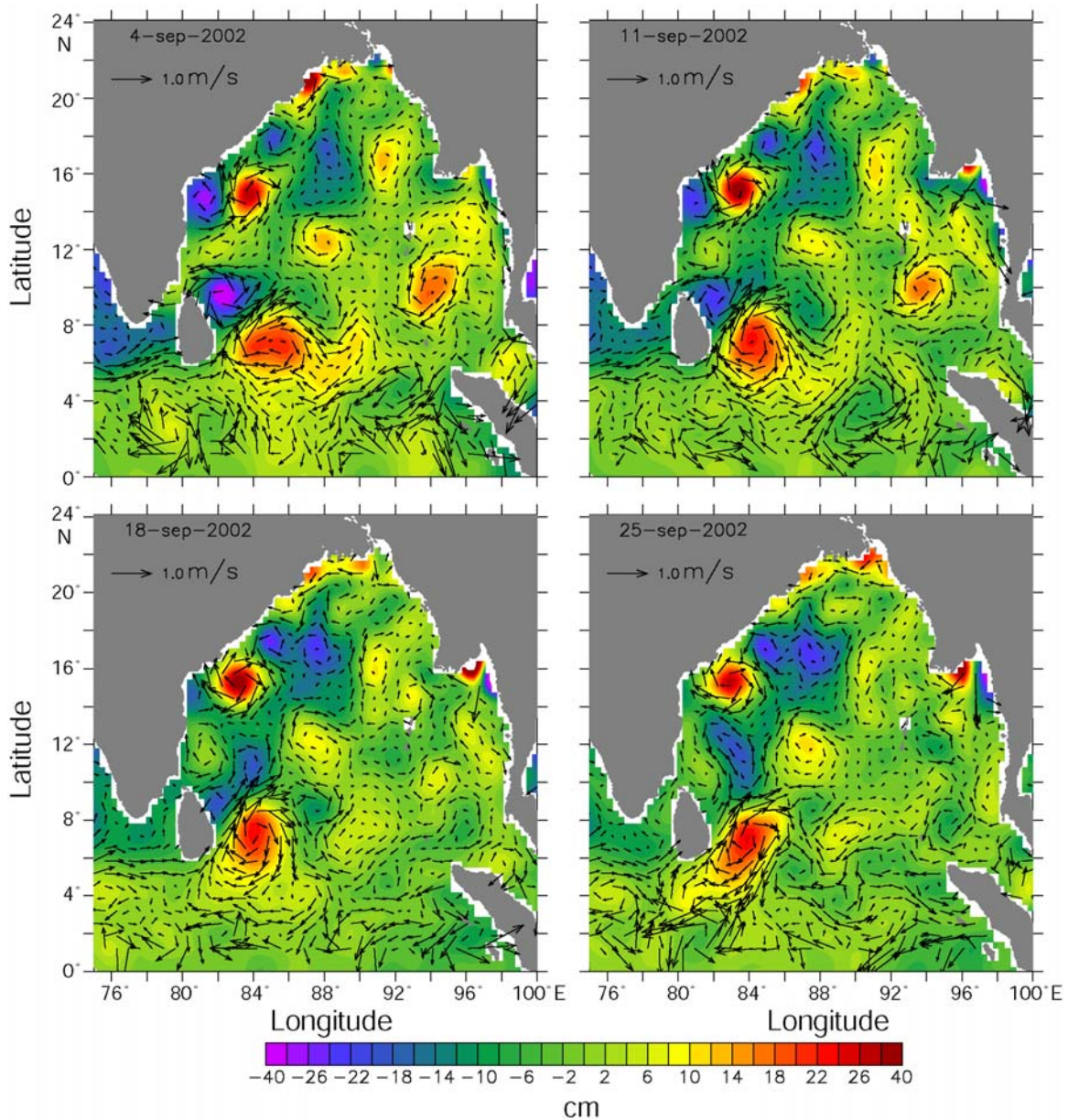


Figure 3.3.3.1. 7-day snap-shots of Topex/Poseidon ERS1/2 merged sealevel anomalies overlaid with geostrophic velocities during September 2002.

September 2002 (Figure 3.3.3.1), which was centered at  $18^{\circ}\text{N}$ ,  $85^{\circ}\text{E}$  and  $17^{\circ}\text{N}$ ,  $88^{\circ}\text{E}$  respectively. By last week of September, these two eddies moved closer (Figure 3.3.3.1). In early October the shipboard measurements sampled the eddy (NCE) centered at  $17^{\circ}\text{N}$ ,  $85^{\circ}\text{E}$  (Figure 3.3.3.2 top left; see Figure 3.2.3.1 for the thermohaline structure). The eddy



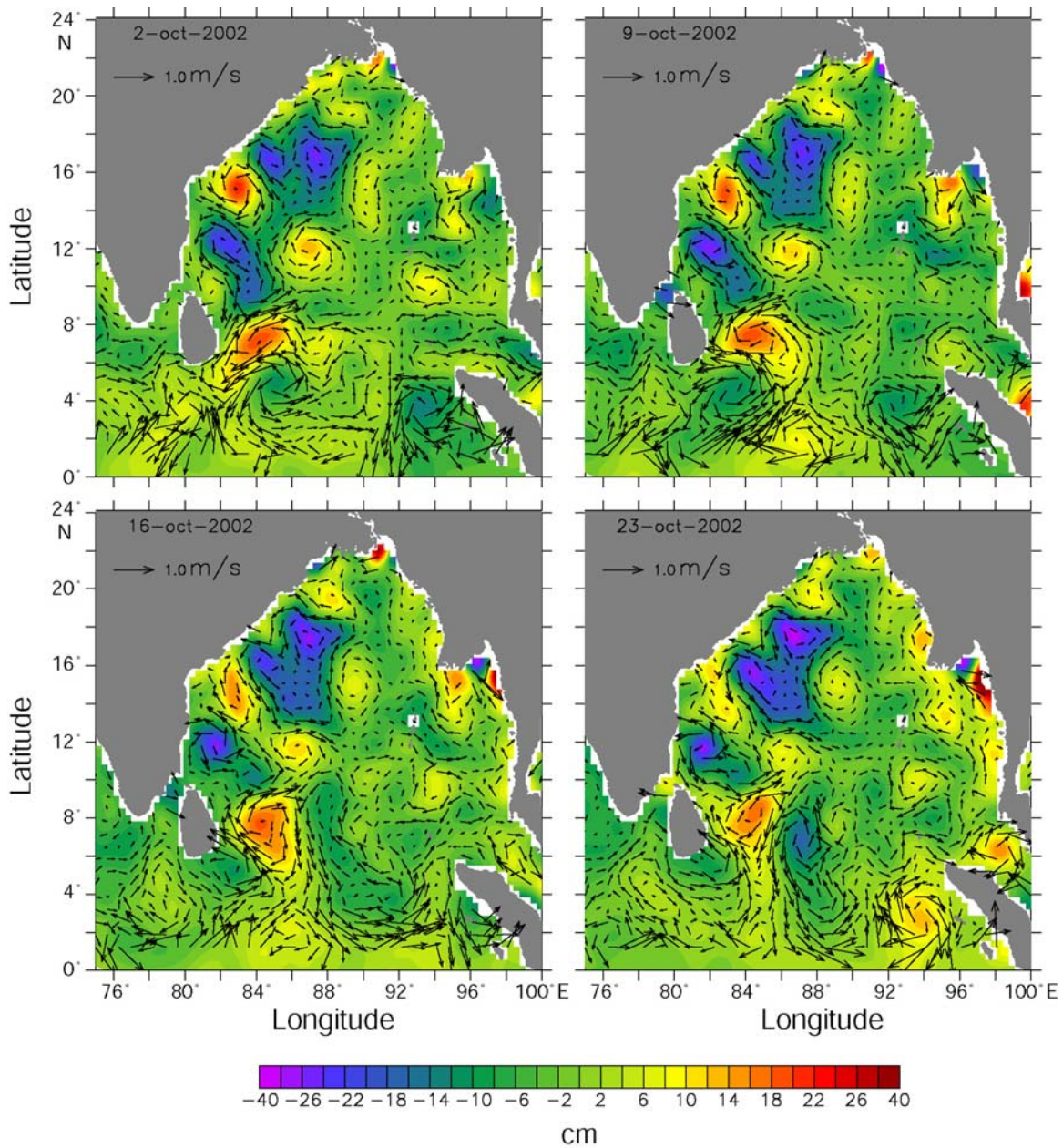


Figure 3.3.3.2. 7-day snap-shots of Topex/Poseidon ERS1/2 merged sealevel anomalies overlaid with geostrophic velocities during October 2002.

centre had a negative sea-level anomaly of 28 cm and geostrophic swirl velocities of 30-40 cm/s along its periphery. Finally both the eddy merged into the cyclonic circulation, which prevailed in the Bay during fall intermonsoon 2002 (Figure 3.3.3.2, bottom left). In the south, the eddy (SCE) centered at 12°N was not discernible during the first week of

September (Figure 3.3.3.1). However, in the third week of September a patch of low sea-level anomaly was seen extending from the northeastern part of Sri Lanka. This patch moved in a northwest direction with time and intensified into a cyclonic eddy (SCE) during October (Figure 3.3.3.2), which was sampled on 9 October 2002 from the ship.

Thus, the sea-level anomaly maps shows that the cyclonic eddies observed in the northern part of the western boundary (NCE), during spring intermonsoon as well as summer monsoon, originated from a meander in the northeastward flowing WBC during Spring intermonsoon. However, at this stage it is difficult to conclude about the origin of NCE during fall intermonsoon from the sea-level anomaly maps. There were two cyclonic eddies observed in the southern part of the western boundary (SCE) during spring and fall intermonsoons respectively. The spring intermonsoon SCE was formed when the anticyclonic circulation offshore of the southern part of the western boundary intensified and approached the coast during the first week of April. However, this feature dissipated within couple of weeks. The SCE seen during fall intermonsoon arises from the intensification of a patch of low sea-level anomaly, which moved from northeastern part of Sri Lanka into the western boundary region during summer. The anticyclonic eddies seen in the thermohaline structure of summer monsoon and fall intermonsoon seems to be the remnant of the large scale anticyclonic circulation that prevails in the BOB during spring intermonsoon. Thus, the hydrographic field along the western boundary of BOB showed the dominance of eddies. The NCE during summer monsoon and spring intermonsoon are generated from the meander in the northeast ward flowing western

boundary current, whereas the SCE during fall intermonsoon appears to have moved from the SLD region into the western boundary of the BOB.

### **3.4. Mechanisms of generation**

Having described the characteristics of the NCE from the *in situ* as well as the satellite data, it is pertinent to examine the potential mechanism/s that could generate eddies during western boundary current regime. Since NCE during spring intermonsoon (NCE-2003) and the summer (NCE-2001) were found to be associated with the meander in the western boundary current, the discussion is focused only to the NCE during the above periods.

The trigger for the eddy generation could be the instability of the western boundary current (WBC). The cross-shore and along-shore dimensions of the WBC in the region of eddy generation are about 150 km and 500 km respectively. A scale analysis of the horizontal motion associated with the WBC showed that  $Lr^2/L^2 \leq O(1)$  [Pedlosky, 1979], where  $Lr$  (~70 Km) is the Rossby deformation radius and  $L$  is the horizontal scales of motion, which suggests the role of baroclinic instability in generating eddies.

From the topography of isopycnals (Figure 3.2.1.1c & Figure 3.2.2.1c) the horizontal dimension of the eddy was found to be approximately 352 km during spring intermonsoon 2003 and about 311 km during summer monsoon (core of the eddy was slightly away from the sampling track). The typical value for first mode internal Rossby



deformation radius ( $L_r$ ) in the northern Bay of Bengal is approximately 70 km (Figure 3.4.1).

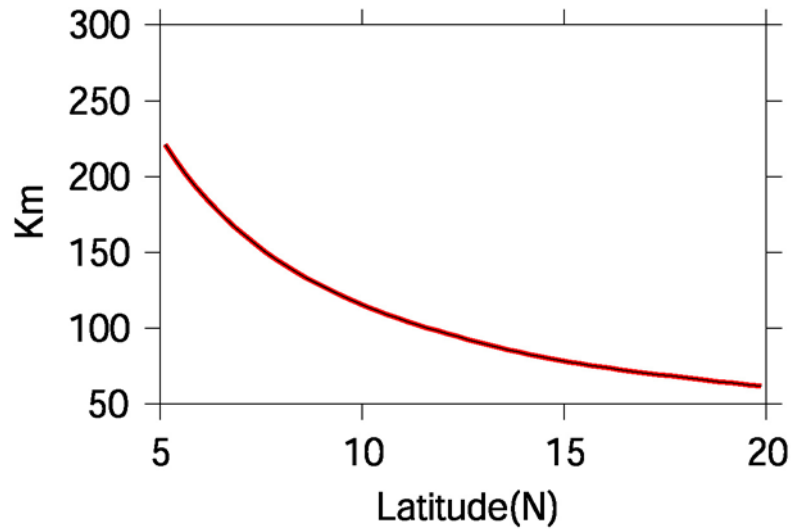


**Figure 3.4.1** Rossby deformation in the BOB along 88°E ( see Chapter 2 for details of computation ).

The wavelength of most unstable baroclinic instability process is given by  $2\pi L_r$  [Stammer and Boning, 1992] and in the northern Bay of Bengal this is about 440 km. From the sea-level anomaly maps the transverse dimension of this eddy was found to be about 430 km. Eddy dimensions obtained from sea-level anomaly maps differed from the hydrography by about 80 km.

However, the computed dimension broadly agrees with the observed one within the resolvable limits of sea-level anomaly ( $\sim 37$  km) and hydrography ( $\sim 150$  km). The agreement between the theoretical and the observed spatial dimensions suggest the role of baroclinic instability of large-scale currents in generating eddies [Kamenkovich *et al.*, 1986]. In the present case, it is the instability associated with the northeastward flowing spring time WBC of the BOB.

The sea-level anomaly maps showed that the meanders in the northeastward flowing WBC forms in early February, in 2003 (Figure 3.3.1.1), and the signatures of cyclonic circulation was seen towards the end of February which becomes fully developed by the end of March (Figure 3.3.1.2). Thus, time span for the meander to develop into a cyclonic circulation is about three-weeks. A similar time-span was found during 2001 as well (Figure 3.3.2.1 & Figure 3.2.2.2).

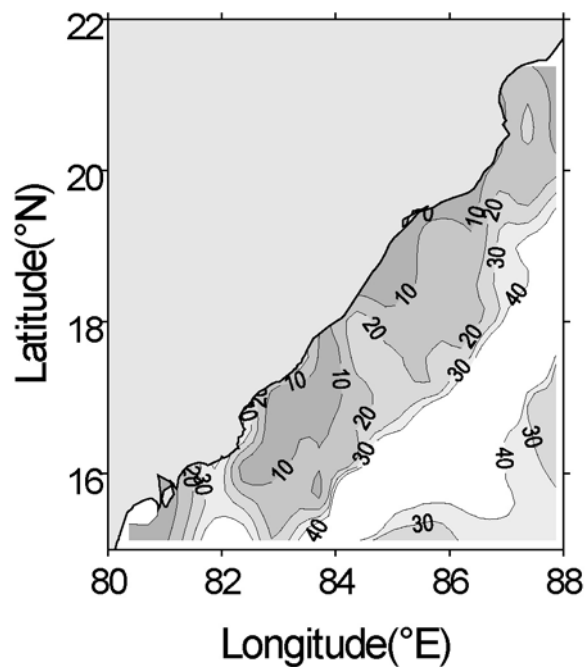


Figure 3.4.2 Baroclinic time scale (days) computed from WOA01 climatology [Conkright *et al.*, 2002] along the region where NCE is formed. See text for details.

Following *Stammer* [1998], a baroclinic time scale  $\sqrt{Ri} / f$  (where *Ri* is the Richardson number, *f* the coriolis parameter) was computed from the WOA01 climatology [Conkright *et al.*, 2002] for 50 to 1000m depth of water column for the northwestern Bay

of Bengal (Figure 3.4.2). The mean vertical shear in the velocity was computed from the cross-shore density differences. However, horizontal density gradient less than  $6 \times 10^{-8}$  was discarded, as the corresponding velocity is too small, of the order of  $10^{-1}$  cm/s in the northwestern region. In the northwestern Bay of Bengal ( $15^{\circ}\text{N}$ - $22^{\circ}\text{N}$ ,  $80^{\circ}\text{E}$ - $88^{\circ}\text{E}$ ) baroclinic time scale during February-March varied between less than 20 days near to the coast to more than 100 days off shore. Thus, the observed time-scale for the meander to form a cyclonic circulation, obtained from sea-level anomaly, falls within the theoretical values in the western boundary region. This time scale is associated with the growth rate of baroclinic eddies [Eady, 1949; Stammer, 1998]. The agreement of the observed time scale with the predicted one suggests, once again, the role of baroclinic instability process in the formation of eddies along the western boundary region of the Bay of Bengal.

An examination of the density structure at 100 m computed from WOA01 climatology [Conkright *et al.*, 2002] reveals the presence of denser waters close to the shore during January and February with strong cross-shore gradients (Figure 3.4.3). The cross-shore density gradient accompanied by vertical shear in the horizontal velocity is a necessary condition for baroclinic instability [Pedlosky, 1979]. The possible mechanisms that can lead to this cross-shore density gradient could be (1) topographic changes, (2) wind forcing, and (3) remote forcing, either individually or in combination.

The topography along the western boundary of the Bay of Bengal from  $15^{\circ}$  to  $20^{\circ}\text{N}$ , obtained from ETOPO data having five-minute resolution showed that the orientation of the coast turns eastward at  $16^{\circ}\text{N}$ .

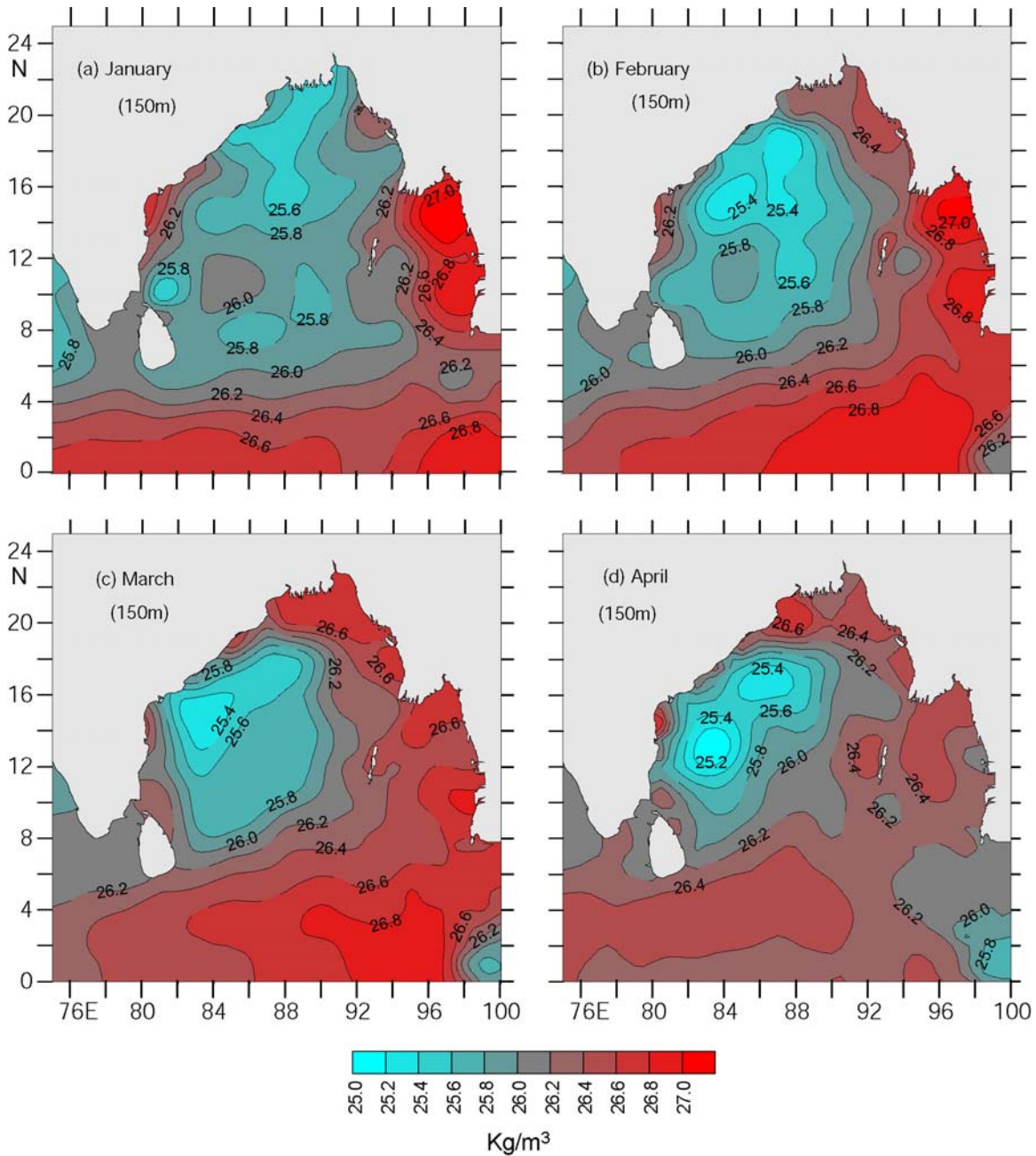


Figure 3.4.3. Basin-wide distribution of monthly mean sigma-t at 150m depth during (a) January, (b) February, (c) March and (d) April derived from WOA01 quarter-degree climatology [Conkright et al., 2002].

The meandering of the northeastward WBC and the resultant eddy formation took place in the vicinity of 20°N during 2001, where as during 2003 the meander formed at about 17°N, which was away from the eastward turn at 16°N. This would mean that topographic change has little contribution to the formation of eddy. Thus, it seems that

along the western boundary of the Bay of Bengal topographic change is not a necessary condition for the formation of eddies.

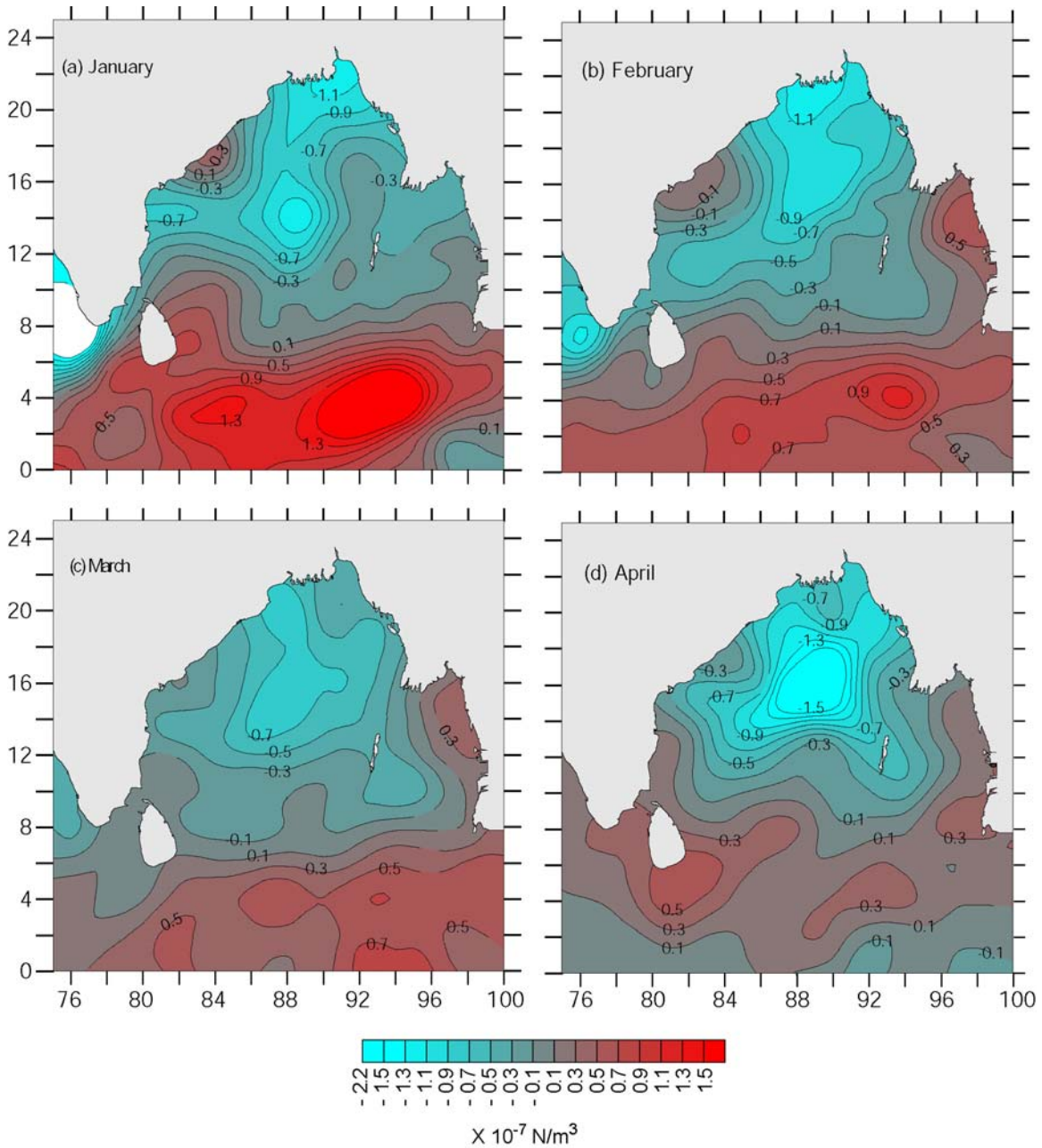


Figure 3.4.4. Curl of wind stress ( $\times 10^{-7}$  N/m<sup>3</sup>) derived from Southampton oceanographic centre monthly mean climatology of wind-stress [Josey *et al.*, 2002]

The basin-wide distribution of monthly mean wind-stress curl computed from SOC climatology [Josey *et al.*, 2002] showed large negative curl in the northern Bay from



January to April having its peak in April (Figure 3.4.4). However, a patch of positive curl was noticed close to the northwestern boundary between 16° and 18°N during January and 14° and 17°N during February.

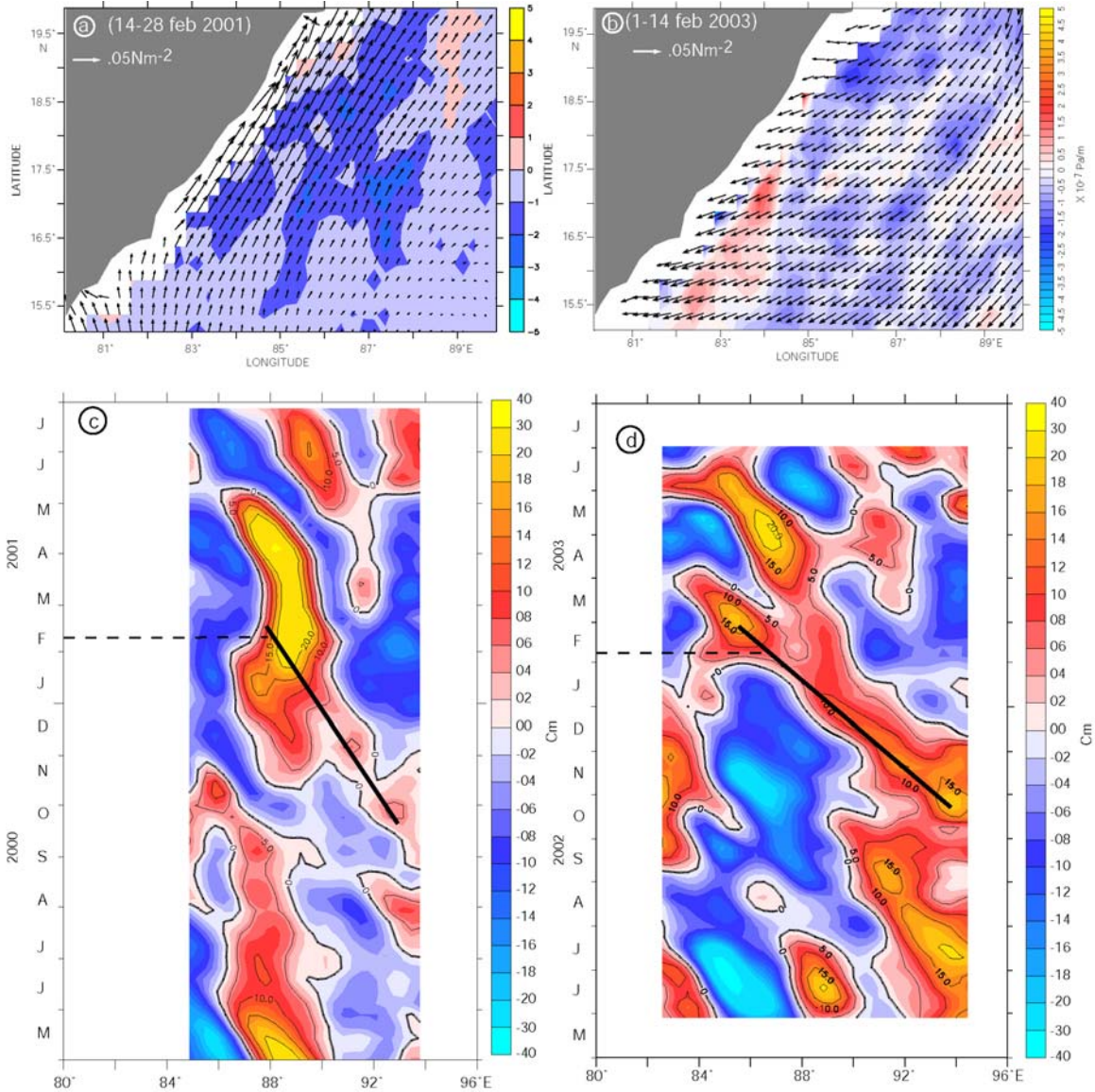


Figure 3.4.5 (a) Curl of wind stress ( $\times 10^{-7}$  Pa/m) derived from QuikSCAT during 1-14 February 2003 and (b) during 14-28 February 2001), (c) zonally de-meaned merged SLA of Topex/Poseidon-ERS 1/2 series of satellites along 19°N (positive values are contoured) during June 2000 to June 2001, (d) along 17°N (positive values are contoured) during June 2002 to June 2003. Bold slanting line indicates the Rossby wave propagation during respective years. Broken line shows the cross-shore SLA gradient which is a result of upwelling along the western boundary and downwelling offshore.

The QuikSCAT wind-stress (Large-Pond method) curl also showed positive curl close to the western boundary (close to the location of eddies) during 2003 and 2001 (Figure 3.4.5, top left and right). In response to this, one would expect large-scale convergence and downwelling of surface water under the negative wind-stress curl, while divergence and upwelling of subsurface waters close to the coast under the positive wind-stress curl. In fact, *Murty and Varadachari* [1968], *Rao et al.* [1986], *Shetye et al.* [1993] and *Rao* [2002] noticed upwelling signatures very close to the coast during spring intermonsoon. In addition, *Rao* [2002] also showed deepening of pycnocline in the offshore region between 15° and 17°N (see Figure 10 of *Rao*, 2002). Thus, wind-forcing is capable of generating the necessary cross-shore density gradient.

A zonally de-meaned SLA along the latitude of eddy formation during 2003 and 2001 showed a westward propagation of high sea-level anomaly (Figure 3.4.5, bottom) which was also clearly seen in the climatology of SLA in the same latitude (Figure 3.4.6) and indicates the propagation of Rossby waves. This Rossby wave can augment the basin-wide negative wind-stress curl in deepening the pycnocline. Thus, the negative wind-stress curl and Rossby wave act in union to deepen the pycnocline in the offshore region, while the positive wind-stress curl shallows the pycnocline close to the coast. This in turn will generate strong cross-shore density gradient, as is evident from Figure 3.4.3, necessary for the baroclinic instability that leads to eddy generation.



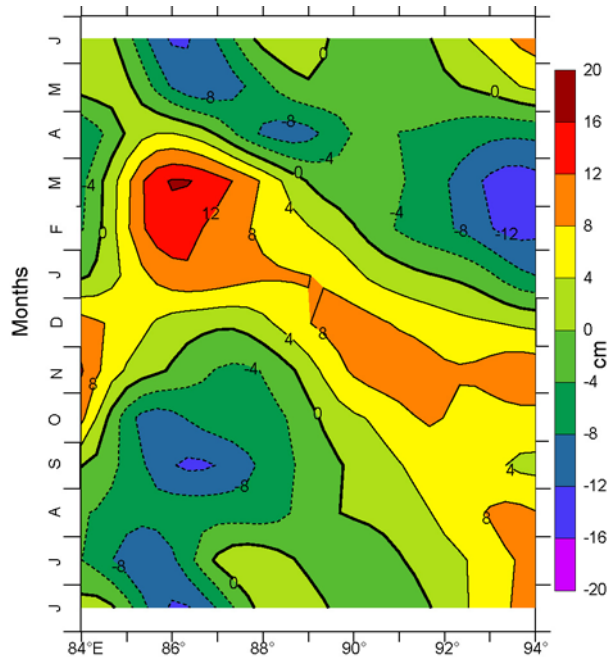


Figure 3.4.6. Time-longitude plot of monthly mean (1992-October to 2004-January) sea-level anomaly climatology derived from merged sea-level anomalies of Topex/Poseidon and ERS 1/2 satellites obtained from AVISO CNES, along 18°N starting from June. See text for details.

### 3.5. Summary

The present chapter deals with the cyclonic eddies observed in the BOB from the thermohaline structure during summer (July-August, 2001), fall intermonsoon (September-October, 2002) and spring intermonsoon (April-May, 2003) along the western boundary and describes its structure, evolution and possible generation mechanisms based on *in situ* and remote sensing data . The doming of isolines in the vertical distribution of temperature/salinity/density manifested the signature of eddy and was most pronounced in the northern part of the western boundary during spring intermonsoon. Accordingly, this eddy depressed the ambient temperature of upper-thermocline by 6°C and increased the near-surface salinity by 0.8 psu. The presence of these cyclonic eddies were confirmed using satellite derived sea-level anomaly maps,

which further indicated that the eddy observed in spring intermonsoon and summer originates as a meander in the WBC. However, the origin of the fall intermonsoon eddy was not clear from the sea-level anomaly maps. These cyclonic eddies encountered in the northern part of the western boundary ( $16^{\circ}$ - $19^{\circ}$ N) in all the three seasons are designated as northern coastal eddy (NCE), while that in the southern part centered at  $14^{\circ}$ N and  $12^{\circ}$ N during spring and fall intermonsoons respectively is designated as southern coastal eddy (SCE). The NCE formed during the WBC regime of 2001 and 2003, had a complex life cycle undergoing offshore-onshore movements, southwestward translation, coalescence and splitting before they finally get dissipated; all of which occurred within a span of approximately 5 months. The time and space scales associated with the NCE during spring and summer suggested the role of baroclinic instability in generating them. With a suite of *in situ* and remote sensing data set, it has been found that a combination of remote and local forcing induced the baroclinic instability along the western boundary. They are 1) the positive wind-stress curl close to the western boundary 2) large negative wind-stress curl in the offshore region, and 3) westward propagating Rossby waves. The positive wind-stress curl close to the western boundary during January-February, between  $14$ - $20^{\circ}$ N, drives divergence and upward Ekman pumping leading to upwelling of subsurface cold waters, while the large negative wind-stress curl in the offshore region combined with westward propagating Rossby waves drives convergence and downwelling of warm surface waters.